Nanoscale design of the local density of optical states

Sandro Mignuzzi,[1, *] Stefano Vezzoli,[1] Simon A. R. Horsley,[2]
William L. Barnes,[2] Stefan A. Maier,[1, 3] and Riccardo Sapienza[1]

[1] *The Blackett Laboratory, Department of Physics,*
Imperial College London, London SW7 2BW, United Kingdom
[2] *Department of Physics and Astronomy, University of Exeter, Exeter EX4 4QL, United Kingdom*
[3] *Chair in Hybrid Nanosystems, Nanoinstitute Munich, Faculty of Physics,*
Ludwig-Maximilians-Universität München, 80799 München, Germany

We propose a design concept for tailoring the local density of optical states (LDOS) in dielectric nanostructures, based on the phase distribution of the scattered optical fields induced by point-like emitters. First we demonstrate that the LDOS can be expressed in terms of a coherent summation of constructive and destructive contributions. By using an iterative approach, dielectric nanostructures can be designed to effectively remove the destructive terms. In this way dielectric Mie resonators, featuring low LDOS for electric dipoles, can be reshaped to enable enhancements of three orders of magnitude. To demonstrate the generality of the method, we also design nanoantennas that enhance the radiated power of a circular dipole, a quadrupole and an arbitrary collection of coherent dipoles. Our concept provides a powerful tool for high-performance dielectric resonators, and affords fundamental insights into light-matter coupling at the nanoscale.

The local density of optical states (LDOS) is the number of electromagnetic modes per unit volume and frequency, at a given point in space. Through Fermi's golden rule, an enhancement of the LDOS implies an increase in the decay rate of an emitter, which is also known as the Purcell effect [1–4]. The LDOS controls the emission, scattering and absorption of light, finding applications in cavity electro-dynamics [5], lasing [6] and solar cells [7]. Traditional cavities, including laser resonators and photonic crystal cavities, modify the LDOS spectrally, and enhance light emission only on resonance with the cavity mode [8]. Due to their large quality factor (Q up to 10^{10} [9]), these microcavities require a stable and precise spectral matching with the emitter.

More recently, nanocavities and nanoantennas have been explored since they sculpt the optical modes down to the near-field [10–12], enabling nanometric optical confinement, without strong spectral bandwidth restrictions [10, 11]. This confinement can be achieved with metal nanostructures where the sub-wavelength localization of light is achieved through the excitation of surface plasmon-polaritons [13], and more recently with high-index dielectric nanostructures which confine light via Mie resonances [14]. Dielectrics are advantageous because they feature minimal absorption losses over broad spectral ranges [14], however, they typically achieve decay rate enhancements that are two orders of magnitude lower [15–18] than their plasmonic counterparts [12]. Despite several proposals to increase the quality factor of dielectric nanocavities [16, 19], their application to controlling the emission of light is still far from optimized.

Previously, high decay rates have been achieved in high optical-field regions, the so-called hotspots [20]. In dielectrics, sub-wavelength hotspots have been achieved in nanogaps [21, 22] where the electric field is boosted, and a decay rate enhancement as high as ≈ 30 has been demon-strated [23, 24]. Recently, the concept of mode matching between the dipole and the plasmonic antenna was introduced and used to provide some guiding principles to optimize the emission [25].

Here we take inspiration from the ideas put forward in Ref. [25] where the LDOS, i.e. a local optical property, is reformulated in terms of a volume property of the fields; we now extend this idea in two ways. First, we go beyond the quasi-static approximation implicit in Ref. [25] and provide a very general approach that can be used to control the local density of states for a variety of sources including: optical, RF and acoustic. Second, our approach provides an iterative design tool based on the Born approximation. Despite the generality of our method, here we focus on the specific case of optical nanoantennas to highlight the power of our new approach and allows us to significantly improve existing designs.

We consider the partial (i.e. directionally dependent) LDOS, $\rho_{\mathrm{p}}(\mathbf{r}_d)$, for an oscillating electric dipole, at position $\mathbf{r}_d$ and along the direction $\mathbf{e}_d$, and we compare it to its free space value, ρ_0. The geometry of the problem is sketched in Fig. 1a, showing a dipole in vacuum, with dipole moment $\mathbf{d}$, in proximity to a dielectric of volume V. The dipolar source field is back-scattered by the dielectric environment, producing a net scattered field $\mathbf{E}_s$ at the site of the dipole. The partial LDOS enhancement, ρ_p/ρ_0, and the radiative decay rate enhancement, γ/γ_0, depend on this back-action as [26, 27]:

$$\frac{\rho_{\mathrm{p}}}{\rho_0} = \frac{\gamma}{\gamma_0} = 1 + \frac{6\pi\epsilon_0}{|\mathbf{d}|^2}\frac{1}{k^3}\mathrm{Im}\left\{\mathbf{d}^* \cdot \mathbf{E}_s(\mathbf{r}_d)\right\} \qquad (1)$$

with ϵ_0 the permittivity in vacuum, k the wavenumber. ρ_0 and γ_0 are the free space LDOS and radiative decay rate respectively. The sources that produce the scattered fields are the induced currents $\mathbf{J}_s$ in the
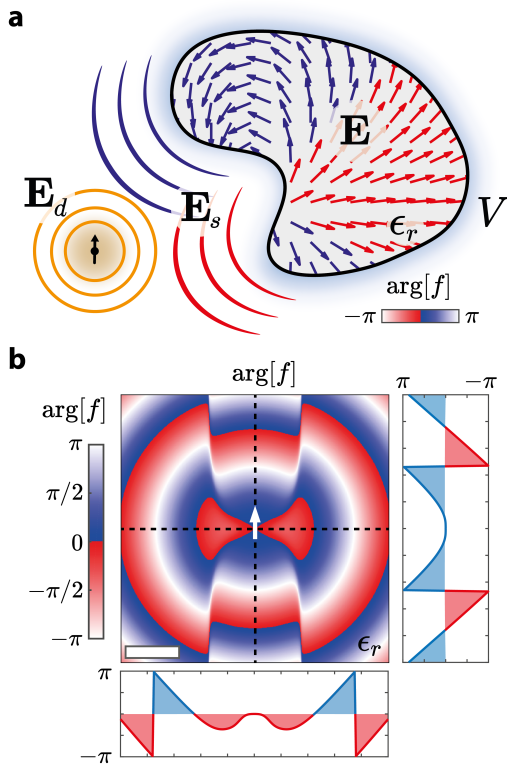
FIG. 1. (a) Sketch of an emitter in vacuum in the proximity of a dielectric structure with permittivity ϵ_r. The arrows in the dielectric represent the field components responsible for increasing (blue) or decreasing (red) the decay rate of the emitter. The type of field component is discriminated by $\arg[f]$ with $f = \mathbf{E}_d \cdot \mathbf{E}$ defined in Eq. 2. (b) A spatial map of $\arg[f]$ for a dipole emitting at $\lambda_0 = 800$ nm in a homogeneous medium of $\epsilon_r = 4$. Scale bar is 200 nm.

dielectric surrounding the emitter. Such currents are related to the field $\mathbf{E}$ inside the dielectric volume by $\mathbf{J}_s = -i\omega\epsilon_0(\epsilon_r - 1)\mathbf{E}$. The reciprocity theorem [26] allows Eq. (1) to be re–written as [SI]:

$$\frac{\gamma}{\gamma_0} = 1 + \frac{6\pi\epsilon_0^2}{|\mathbf{d}|^2} \frac{1}{k^3} \, \text{Im}\left[\int_V d^3\mathbf{r}(\epsilon_r(\mathbf{r}) - 1)\, \mathbf{E}_{d*}(\mathbf{r}) \cdot \mathbf{E}(\mathbf{r}) \right] \tag{2}$$

where the integral extends over the volume V of the dielectric, ϵ_r is assumed real, and $\mathbf{E}_{d*}$ is the field of the time–reversed dipole moment in free space (i.e. $\mathbf{E}_{d*} = \omega^2\mu_0\mathbf{G}_0(\mathbf{r}, \mathbf{r}_d) \cdot \mathbf{d}^*$, with $\mathbf{G}_0$ the free space Green function). Note that, for a linear dipole, there is no useful distinction between $\mathbf{E}_d$ and $\mathbf{E}_{d*}$. The derivation is further detailed in the Supplementary Information [SI], where an equivalent Green function formalism approach is also described. As illustrated in Fig. 1a, the decay rate is determined by the coherent contributions of spatially distinct field elements in the dielectric medium. Each field element is responsible for driving or damping the emitter (blue and red respectively in Fig. 1a), depending
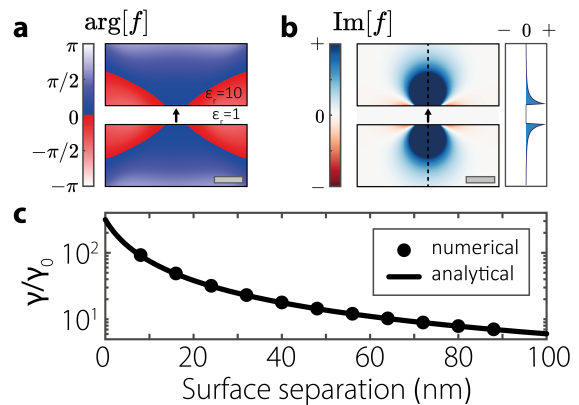

FIG. 2. LDOS between two infinite parallel plates of $\epsilon_r = 10$, for a perpendicular dipole ($\lambda_0 = 800$ nm) in the middle of the air gap. (a) The spatial distribution of $\arg[f]$, (b) of $\text{Im}[f]$ and the relative cross-section along the dotted line, and (c) decay rate enhancement as a function of the separation between the plates calculated both analytically (line) [SI] and solving Eq.2 numerically. Scale bar is 50 nm.

on the sign and amplitude of $\text{Im}[\mathbf{E}_{d*} \cdot \mathbf{E}] = \text{Im}[f]$, where we define $f = \mathbf{E}_{d*} \cdot \mathbf{E}$. The amplitude of f, i.e. $|f|$, can be controlled by matching the (vacuum) field distribution of the emitter $|\mathbf{E}_{d*}|$ with that of the induced fields $|\mathbf{E}|$, as shown in ref. [25]. On the other hand, the phase of f, i.e. $\arg[f]$, determines the sign of $\text{Im}[f]$, and thus the enhancement or suppression of the radiative decay. Regions of dielectric where $\arg[f] \in [0, \pi]$ (i.e. $\text{Im}[f] > 0$) (shown blue) give a positive contribution, whereas regions where $\arg[f] \in [-\pi, 0]$ (i.e. $\text{Im}[f] < 0$) (shown red) give a negative contribution, and therefore should be removed if the decay rate is to be enhanced.

In Fig. 1b we show $\arg[f]$ for a dipole in a homogeneous medium, calculated analytically [SI]. The phase of the fields is relevant even within the near-field region of the dipole, where one would assume optical retardation is negligible. As illustrated by the cross sections, in the near-field (within a distance $\sim \lambda_0/2n$, which is the size of the scale bar in Fig. 1b) $\arg[f]$ is positive along the longitudinal direction, but negative along the transversal direction. The complex function f is key to the nanoscale design of structures for LDOS control. For LDOS enhancement, the damping contributions (red regions in Fig. 1b) to the integral in Eq. 2 could be removed by physically removing dielectric material in the regions where $\arg[f] \in [-\pi, 0]$. The fields and the function f can then be re-calculated and the process repeated iteratively so as to optimize the degree of enhancement.

We first test this concept on a simple vacuum/air nanogap surrounded by two dielectric half-spaces with a high refractive index [22, 28], as illustrated in Fig. 2, which can be solved analytically [SI]. We consider a dipole source (wavelength $\lambda_0 = 800$ nm) located at mid-gap, and oriented perpendicular to the interfaces. The
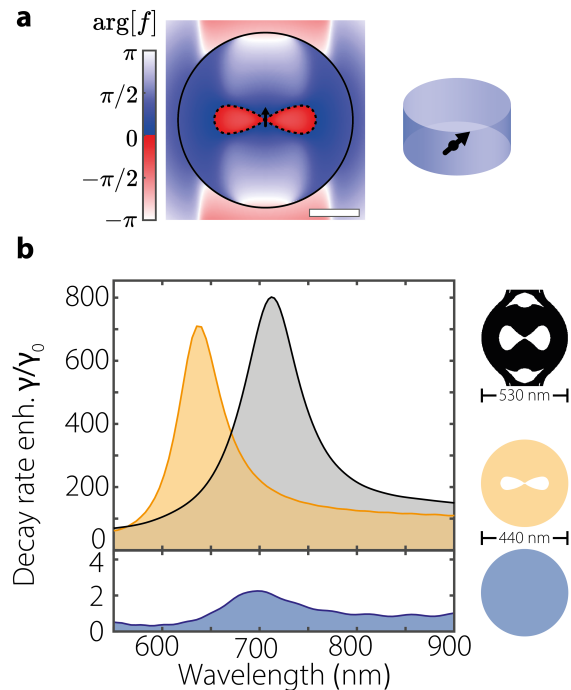
a

b

FIG. 3. (a) Phase map ($\arg(f)$) of a GaP nanodisk resonator (440 nm diameter, 50 nm height), when excited by a dipole ($\lambda = 700$ nm) in its center at mid-height, surrounded by vacuum. The dotted line indicates the out-of-phase components that are removed to implement the phase design. Scale bar is 150 nm. (b) Decay rate enhancement for a full nanodisk resonator (blue), a perforated one (yellow) and a resonator designed by an iterative procedure (black) .

permittivity is $\epsilon_r = 1$ at the dipole position and $\epsilon_r = 10$ within the dielectric plates. We numerically calculate $f(\mathbf{r})$ over the volume of the dielectric, using FDTD [SI], as prescribed by Eq. 2. The spatial distributions of $\arg[f]$ and $\mathrm{Im}[f]$, for a gap width of 32 nm, are shown in Fig. 2a and b respectively. As seen in Fig. 2b, the sign of $\mathrm{Im}[f]$ is strongly correlated with the distribution of the phase (Fig. 2a), whereas the amplitude of $\mathrm{Im}[f]$ becomes stronger in the proximity of the dipole, where the field is highest. The decay rate calculated numerically are in very good agreement with analytically [SI], as shown in Fig. 2c. As shown in Fig. 2b, $\mathrm{Im}[f]$ is mostly positive (blue), leading to a strong enhancement of the decay rate: the nanogap is effectively removing regions of dielectric where polarization currents would give a negative contribution to the LDOS (red).

We now discuss the design of nanoresonators, compatible with current nanofabrication technology, for the efficient enhancement of the decay rate. We consider a simple resonator geometry, a high index dielectric nanodisk with a Mie resonance, which has been recently demonstrated to effectively confine radiation [29, 30]. Such subwavelength structures typically have low quality factors (Q< 30) [19], confine the field to a volume of $\sim \lambda^3$, and

consequently feature poor decay rate enhancements. In Fig. 3a we illustrate a spatial map of $\arg[f]$ for a gallium phosphide (GaP) dielectric nanodisk, excited at its anapole resonance by a dipole at the center of the disk, at half its height. The destructive contributions (red) to the LDOS in Fig. 3a, prevents large decay rate enhancements. As shown in of Fig. 3b (blue curve) the decay rate enhancement is peaked at the anapole resonance ~ 700 nm, and is never larger than ~ 2 times (2.2 on resonance). When the dielectric material with negative $\arg[f]$, i.e. the red double-hole region between the dotted lines in Fig. 3a, is removed, the decay rate increases by up to $\gamma/\gamma_0 = 708$, as illustrated in Fig.3b (yellow curve). The blue-shift of the resonance is due to a lower effective refractive index [SI]. In our design the double-hole is connected via a nanogap of 8 nm, which is feasible with He focused ion beam drilling [31].

This nanocavity design, based on a visual inspection of $\arg[f]$, perturbs the modes of the structure so that the distribution of $\arg[f]$ is no longer as it was in Fig. 3a before the introduction of the holes. The design can be improved further through an iterative procedure where for each step the permittivity ϵ is gradually changed by an infinitesimal amount $\pm\delta\epsilon$, depending on whether $\mathrm{Im}[f]$ is positive or negative; all points in the dielectric volume surrounding the dipole emitter are considered in this way. By using a Born approximation it can be demonstrated [SI] that the change in the integral of Eq. 2 is proportional to $\delta\epsilon\,\mathrm{Im}\left[\mathbf{E}_*(\mathbf{r})\cdot\mathbf{E}(\mathbf{r})\right]$, where $\mathbf{E}_*$ is the total electric field due to the time reversed dipole moment $\mathbf{d}^*$ [SI] (again, the distinction between $\mathbf{E}$ and $\mathbf{E}_*$ can be ignored for a linear dipole). The electric field is numerically recalculated after each change to the permittivity profile, so that the LDOS is optimized at $\mathbf{r}_d$, and the final distribution of currents serve to enhance the emission ($\arg[f] > 0$) as much as possible. The graded index resulting from the optimization is then converted to a binary index, for air (ϵ_r=1) and GaP (ϵ_r=10) so as to enable implementation with a homogeneous dielectric. By using this iterative method, a GaP slab is transformed into a closed ring-like structure, shown in black in the inset of Fig. 3b. This is similar to the nanodisk with the eight-shaped holes that we discussed previously (yellow), but with a further boost of γ/γ_0 to ~ 800. Interestingly, this shape is strongly reminiscent of the phase distribution already encountered in Fig. 1b, which reenforces our interpretation of the optimization procedure as a *phase design*. Note that in both cases the mode of the antenna is weakly perturbed and retains a Q of around 10 [SI]. The decay rate could be further increased with a double-tip with a smaller radius of curvature or by increasing the index contrast. The structures shown in Fig. 3b carry a strong resemblance to structures already deployed in nanophotonics, such as bow-tie antennas [24], double hole apertures [32, 33], dielectric slots [22] and pointed probes used in nanospectroscopy [34–36]. The
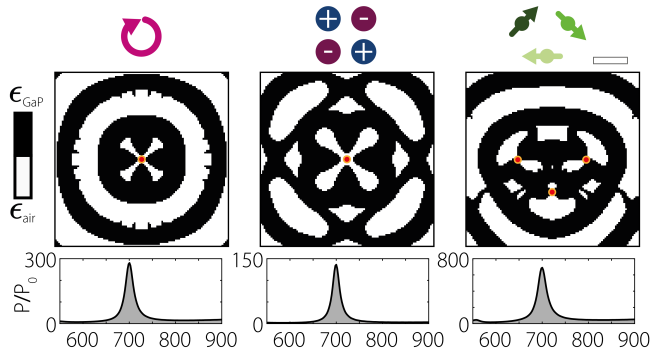
FIG. 4. Design of nanocavities for different sources: circular dipole (a), quadrupole (b), three coherent dipoles (c). The nanoresonators are designed starting from a 50 nm GaP slab, and optimized for a wavelength of 700 nm. Scale bar is 200 nm. The radiated power enhancement P/P_0 is shown in the bottom panels.

experimental success of this range of nanostructures can thus be re-interpreted in the light of our model as a result of the phase distribution in the medium surrounding the dipole. Interestingly, our approach also rationalizes the designs resulting from computationally expensive methods, such as genetic algorithms [37] and inverse designs based on iterative methods [38].

Finally, we illustrate the generality and versatility of our design approach by considering a few non trivial examples beyond the simple case of a single dipole emitter. Fig. 4 illustrates the results of the optimization procedure for a circular dipole (a), a quadrupole point-like emitter (b) and a collection of three coherent dipole emitters located at the vertices of a triangle (c). The nanoantenna design is obtained, like before, by gradually changing the refractive index of an infinite 50 nm thick slab of GaP, within a region of 1×1 μm^2, in order to reduce the out-of-phase components. The Purcell enhancement obtained for the final structures is illustrated in the lower panel of Fig. 4: it reaches a maximum of 280 for the circular antenna and of 135 for the quadrupole antenna, whereas for the three dipole system the radiated power increases by 680 times.

In conclusion, we described a design route for enhancing the LDOS and the radiative decay rate in dielectric nanoresonators based on the spatial distribution of the phase of the induced polarization currents. This is intuitive, versatile and computationally efficient. We obtain decay rate enhancements of 800 for an electric dipole in an improved Mie resonator and similar values for more complex architectures, i.e. circular dipoles, quadrupoles and ensembles of coherent emitters. The method can be extended to lossy dielectrics, plasmonic materials, and is valid also for larger structures, as for example nanoantennas embedded in micro-resonators [39]. In particular, the coherent design can improve nanocavities for weakly emitting point sources, such as magnetic and

multipole molecular transitions, or for acoustics [3] and elastic waves [4]. Extreme LDOS enhancements have important applications for single-molecule spectroscopy and sensing, and open a path towards room temperature quantum coherence for nanoscale quantum optics, strong coupling and single photon non-linearities.

* s.mignuzzi@imperial.ac.uk
[1] M. Fox, Quantum optics: an introduction (Oxford Master Series in Physics, New York, 2006).
[2] E. M. Purcell, Physical Review 69 (1946).
[3] M. Landi, J. Zhao, W. E. Prather, Y. Wu, and L. Zhang, Physical Review Letters 120, 114301 (2018).
[4] M. K. Schmidt, L. G. Helt, C. G. Poulton, and M. J. Steel, Physical Review Letters 121, 064301 (2018).
[5] H. Groß, J. M. Hamm, T. Tufarelli, O. Hess, and B. Hecht, Science Advances 4, eaar4906 (2018).
[6] T. Pickering, J. M. Hamm, A. F. Page, S. Wuestner, and O. Hess, Nature Communications 5, 1 (2014).
[7] H. A. Atwater and A. Polman, Nature Materials 9, 205 (2010).
[8] S. Noda, M. Fujita, and T. Asano, Nature Photonics 1, 449 (2007).
[9] T. Asano, Y. Ochi, Y. Takahashi, K. Kishimoto, and S. Noda, Optics express 25, 1770 (2017).
[10] A. F. Koenderink, ACS Photonics 4, 710 (2017).
[11] R. Chikkaraddy, B. de Nijs, F. Benz, S. J. Barrow, O. A. Scherman, E. Rosta, A. Demetriadou, P. Fox, O. Hess, and J. J. Baumberg, Nature 535, 127 (2016).
[12] G. M. Akselrod, C. Argyropoulos, T. B. Hoang, C. Ciracì, C. Fang, J. Huang, D. R. Smith, and M. H. Mikkelsen, Nature Photonics 8, 835 (2014).
[13] S. Maier, Plasmonics: fundamentals and applications (Springer Verlag, New York, 2007).
[14] A. I. Kuznetsov, A. E. Miroshnichenko, M. L. Brongersma, Y. S. Kivshar, and B. Lukyanchuk, Science 354, 846 (2016).
[15] X. Zambrana-Puyalto and N. Bonod, Physical Review B 91, 1 (2015).
[16] A. Krasnok, S. Glybovski, M. Petrov, S. Makarov, R. Savelev, P. Belov, C. Simovski, Y. Kivshar, A. Krasnok, S. Glybovski, M. Petrov, and S. Makarov, Applied Physics Letters 108, 211105 (2016).
[17] R. Regmi, J. Berthelot, P. M. Winkler, M. Mivelle, J. Proust, F. Bedu, I. Ozerov, T. Begou, J. Lumeau, H. Rigneault, M. F. García-Parajó, S. Bidault, J. Wenger, and N. Bonod, Nano Letters 16, 5143 (2016).
[18] J. Cambiasso, G. Grinblat, Y. Li, A. Rakovich, E. Cortés,

and S. A. Maier, Nano Letters **17**, 1219 (2017).

[19] M. V. Rybin, K. L. Koshelev, Z. F. Sadrieva, K. B. Samusev, A. A. Bogdanov, M. F. Limonov, and Y. S. Kivshar, Physical Review Letters **119**, 243901 (2017).

[20] V. Rutckaia, F. Heyroth, A. Novikov, M. Shaleev, M. Petrov, and J. Schilling, Nano Letters **17**, 6886 (2017).

[21] V. R. Almeida, Q. Xu, C. A. Barrios, and M. Lipson, Optics Letters **29**, 1209 (2004).

[22] J. T. Robinson, C. Manolatou, L. Chen, and M. Lipson, Physical Review Letters **95**, 143901 (2005).

[23] P. Kolchin, N. Pholchai, M. H. Mikkelsen, J. Oh, S. Ota, M. S. Islam, X. Yin, and X. Zhang, Nano Letters **15**, 464 (2015).

[24] H. Choi, M. Heuck, and D. Englund, Physical Review Letters **118**, 223605 (2017).

[25] T. Feichtner, S. Christiansen, and B. Hecht, Physical Review Letters **217401**, 1 (2017).

[26] L. Novotny and B. Hecht, Principles of Nano-Optics (Cambridge University Press, New York, 2006).

[27] A. Cazé, R. Pierrat, and R. Carminati, Physical Review Letters **110**, 1 (2013).

[28] Y. C. Jun, R. M. Briggs, H. A. Atwater, and M. L. Brongersma, Optics Express **17**, 7479 (2009).

[29] A. E. Miroshnichenko, A. B. Evlyukhin, Y. F. Yu, R. M. Bakker, A. Chipouline, A. I. Kuznetsov, B. Luk'yanchuk, B. N. Chichkov, and Y. S. Kivshar, Nature Communications **6**, 8069 (2015).

[30] Y. Yang, V. A. Zenin, and S. I. Bozhevolnyi, ACS Photonics **5**, 1960 (2018).

[31] F. Fang and Z. Xu, in Handbook of Manufacturing Engineering and Technolog, edited by A. Y. C. Nee (Springer London, London, 2015) pp. 1279–1315.

[32] R. Regmi, A. A. Al Balushi, H. Rigneault, R. Gordon, and J. Wenger, Scientific Reports **5**, 1 (2015).

[33] A. Gondarenko and M. Lipson, Optics Express **16**, 17689 (2008).

[34] M. Sanz-Paz, C. Ernandes, J. U. Esparza, G. W. Burr, N. F. Van Hulst, A. Maitre, L. Aigouy, T. Gacoin, N. Bonod, M. F. Garcia-Parajo, S. Bidault, and M. Mivelle, Nano Letters **18**, 3481 (2018).

[35] S. Mignuzzi, F. Huang, D. Roy, and D. Richards, The Journal of Physical Chemistry C **121**, 18800 (2017).

[36] J. Berthelot, S. S. Aćimović, M. L. Juan, M. P. Kreuzer, J. Renger, and R. Quidant, Nature Nanotechnology **9**, 295 (2014).

[37] A. Gondarenko, S. Preble, J. Robinson, L. Chen, H. Lipson, and M. Lipson, Physical Review Letters **96**, 29 (2006).

[38] J. Lu, S. Boyd, and J. Vučković, Optics Express **19**, 10563 (2011).

[39] S. Hu, M. Khater, R. Salas-Montiel, E. Kratschmer, S. Engelmann, W. M. J. Green, and S. M. Weiss, Science Advances **4**, eaat2355 (2017).